3rd URSI AT-AP-RASC, Gran Canaria, 29 May – 3 June 2022

Global Distribution of Energetic Electron Precipitation at Low Earth Orbit from ELFIN Observations

Murong Qin * (1, 2), Wen Li (1), Qianli Ma(1,3), Xiao-Chen Shen(1) and Luisa Capannolo (1)
(1) Center for Space Physics, Boston University, Boston, Massachusetts, USA.
(2) Cooperative Programs for the Advancement of Earth System Science, UCAR, Boulder, Colorado, USA.
(3) Department of Atmospheric and Oceanic Sciences, University of California, Los Angeles, California, USA.

Abstract

Precipitation into the upper atmosphere has been suggested as an important loss process of radiation belt electrons. However, previous measurements of energetic electron precipitation at Low-Earth-Orbit (LEO) either have a coarse resolution in pitch angle and energy or suffer from contamination of ions and penetrating particles. In this study, the global distribution of precipitating and atmospheric backscattered energetic electrons parameterized by geomagnetic activity is statistically investigated using recent data (March 2020 through June 2021) from the Electron Loss and Fields Investigation (ELFIN) CubeSat mission. Stronger electron precipitation and a higher ratio of precipitating to trapped electrons are observed during higher AE for a broad range of energies (~60 keV – ~1 MeV). Results also demonstrate that pitch angle scattering by whistler mode chorus waves accounts for main features of the low energy electron precipitation during various geomagnetic conditions. Electron precipitation at relativistic energies (> ~1 MeV) shows good consistency with current sheet scattering in location and lower correlation with EMIC waves on the duskside, which have been proposed to be responsible for rapid radiation belt electron loss. The LEO observations with high pitch angle resolution in this study provide new insights into the understanding of physical mechanisms that determine the precipitation rate from the magnetosphere into the atmosphere.

1. Introduction

Precipitation into the atmosphere is one of the most important loss mechanisms of radiation belt electrons. Energetic electron precipitation can be driven by various processes, including pitch angle scattering by plasma waves [1, 2] and field-line curvature scattering [3].

Theoretical calculation of electron precipitation has been previously performed; however, the electron precipitation processes and the associated loss rates are still not well understood due to a lack of adequate conjugated wave observations near the equatorial plane and the uncertainties of model calculation caused by assumptions and input parameters. Direct measurements of electron pitch angle distributions near the loss cone are essential to evaluate the underlying physical processes (e.g., pitch angle scattering by plasma waves or other processes). However, the loss cone at the equator is too narrow to be resolved by near-equatorial satellites. In contrast, the loss cone is significantly larger at low altitude, potentially allowing for highly resolved measurements of both trapped and precipitating electron fluxes. Previous measurements of energetic electron precipitation at LEO either have a coarse resolution in pitch angle or suffer from contamination of ions and penetrating particles, thus an accurate estimate of the electron precipitation and the associated physical mechanism are still not available. Additionally, the measurement of backscattered electrons at LEO is also important, not only because they are crucial for understanding the particle and energy deposition in the upper atmosphere, but also because they may contribute to the electron precipitation in the conjugate hemisphere, which could complicate the quantification of precipitating rate and the underlying mechanisms.

In this work, we use electron measurements from the ELFIN mission [4] to evaluate the global distribution of the energetic electron precipitation at LEO and examine its dependence on geomagnetic activity.

2. ELFIN Data Analysis

2.1 Instrumentation

The ELFIN mission was launched in September 2018 and consists of two identical CubeSats (ELFIN-A, B) that are orbiting around the Earth in nearly circular low altitude (450 km) orbits, with an orbital period of ~90 min, spin period about 3s and inclination of ~93°. The energetic particle detector for electrons (EPD-E) measure electrons over 50 keV – 5 MeV in 16 energy channels with energy resolution of $\Delta E/E < 40\%$ and a full 360° field of view. The spin axis of each satellite is maintained perpendicular to the orbital plane, providing full pitch-angle resolution of electrons twice per spin. ELFIN is also designed to prevent contamination by penetrating particles and ion contaminations, allowing for an accurate measurement of electrons.

2.2 Energetic electron distribution observed by ELFIN

Figure 1 shows an example of electron observations from ELFIN-B during moderate geomagnetic conditions on March 06, 2021 (Figures 1a–1b). Significant fluxes are observed for trapped electrons with energies up to 2–3 MeV (Figure 1c). The first patch of high trapped energetic electron fluxes at *L*-shell of 3.6–8.7 before 0707 UT in Figure 1c corresponds to the outer radiation belt region [4]. The trapped flux intensified several times from 0704 to 0705 UT (times 1, 2, and 3). The downward-going electron fluxes (precipitation) in Figure 1d and upward-going electron (backscattered) fluxes in Figure 1f show a similar trend to the trapped fluxes but with a lower flux level. The precipitating electrons are also clearly seen in pitch-angle spectra over the various energy ranges displayed in Figures 1h-1k. To better quantify the precipitation and the backscattered level, we examine the ratio of precipitating to trapped flux in Figure 1e and the ratio of backscattered to trapped flux in Figure 1g. During most of the time, both the precipitation and the backscattered fluxes are at a low but non-negligible level. At time 1, the precipitation only occurs from 60 keV to 200 keV and the precipitating ratio decreases as the energy increases. This suggests that the resonant interactions dominate at low energies and the precipitation could potentially be driven by whistler mode waves. At times 2 and 3; however, the precipitating ratio increases with energy (Figure 1e). At time 2, the intensification of the precipitating ratio is observed only above 200 keV with a maximum value of 1.0 at 2 MeV. Energetic electron precipitation with such feature is likely to be driven by EMIC waves. At time 3, the intensification of the precipitating ratio is observed from 60 keV to 3 MeV. Combining with the fact that precipitation is very localized in space, this is also likely driven by EMIC waves. The backscattered-to-trapped electron flux ratio also intensified at times 2 and 3, while it does not increase as the energy increases. This might be due to the fact that the high-energy electrons are not as easily scattered back out by the atmospheric constitutes as the low-energy electrons.

To statistically evaluate the distribution of energetic electron precipitation as well as the precipitating-to-trapped flux ratios on a global scale, we adopted ELFIN measurements of energetic electrons from March 2020 through June 2021 and sorted them by the AE index.

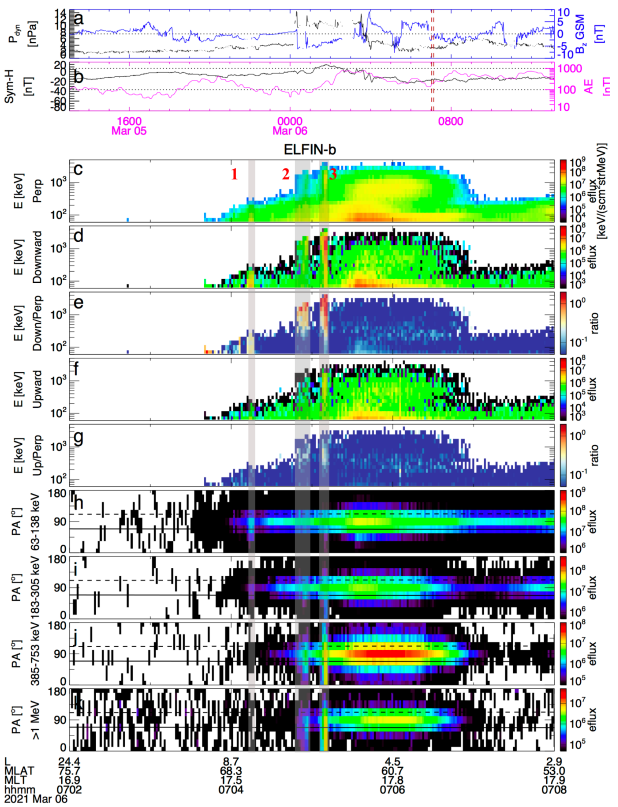

Figure 1. An example of energetic electrons observed by ELFIN on March 06, 2021. (a) solar wind conditions, including solar wind dynamic pressure and interplanetary magnetic field $\boldsymbol{B_z}$ component; (b) geomagnetic conditions, including Sym-H and AE indices. Bottom panels show observations from ELFIN, showing energy spectrograms of the (c) perpendicular electron energy flux, (d) downward-going electron energy flux, (e) the ratio of the downward-going electron energy flux to the perpendicular energy flux, (f) upward-going electron energy flux, (g) the ratio of the upward-going electron energy flux to the perpendicular energy flux, respectively. (h–k) Electron pitch-angle distribution for energies of 63–138, 183–305, 385–753, and > 1,000 keV. Solid and dashed lines in panels h–k demarcate the bounce loss cone and anti-loss cone based on the IGRF magnetic field model at the given the spacecraft location and altitude.

3. Statistical Results

We performed a statistical analysis of the data from both ELFIN-A and ELFIN-B over March 2020-June 2021. The statistical results are shown in Figure 2 (63 keV) and Figure 3 (1 MeV).

Figure 3 shows the global distribution of 63 keV electron fluxes observed at *L*-shells between 3 and 10 categorized by different AE levels at different pitch angles. Electron flux at 63 keV depends strongly on AE index with much stronger intensity during higher geomagnetic activity. The peak intensity locates from dawn to noon. The MLT

distribution of the electron flux measured by ELFIN is roughly consistent with the fluxes of $E > 100$ keV electrons measured by POES [6]. However, the flux has a peak from dawn to noon rather than the nightside. This is consistent with the global distribution of chorus waves [7] that can drive pitch angle scattering of energetic electrons below hundreds of keV.

It is also worth noting that trapped electrons are more confined to the lower L shells on the nightside and extend to higher L shells on the dayside, while precipitating electrons are mainly distributed at $L > \sim 5$. This may be caused by the drift shell splitting effect. It is evident that both the precipitation ratio and the backscattering ratio increases during higher geomagnetic activity level. The increase in precipitating ratio (Figure 3d) during higher geomagnetic activity is consistent with the increasing chorus wave intensity. The backscattering ratio (Figure 3e) overall increases during higher AE when the precipitating ratio is high except at high L shells (8-10), which needs a further detailed examination.

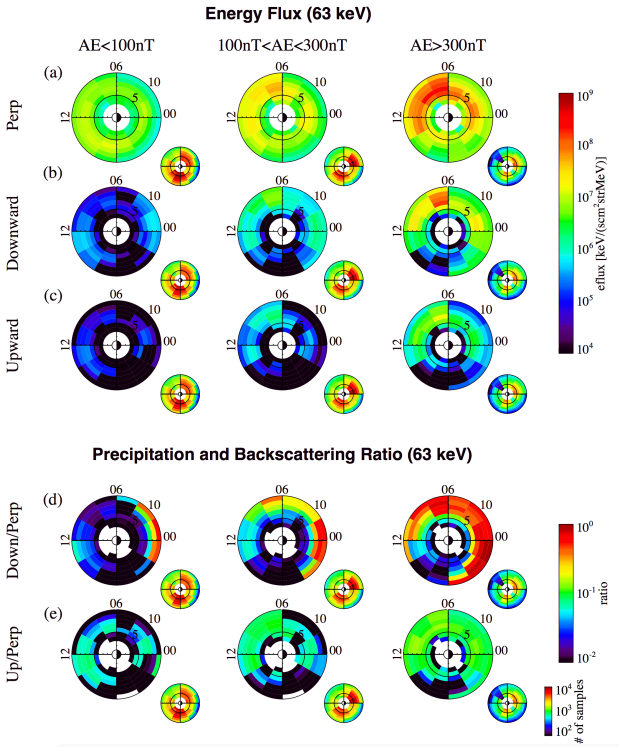

Figure 2. Global distribution of trapped, precipitating and backscattered electrons at 63 keV observed at L shells between 3 and 10 categorized by AE index. (a) Trapped energy flux (b) downward-going (precipitating) electron energy flux, (c) upward-going (backscattered) electron energy flux, (d) the ratio of the downward-going electron energy flux to the perpendicular energy flux and (e) the ratio of the upward-going electron energy flux to the perpendicular energy flux. The larger plots show the energy flux (a–c) and the ratio (d–e). The smaller plots show the number of samples.

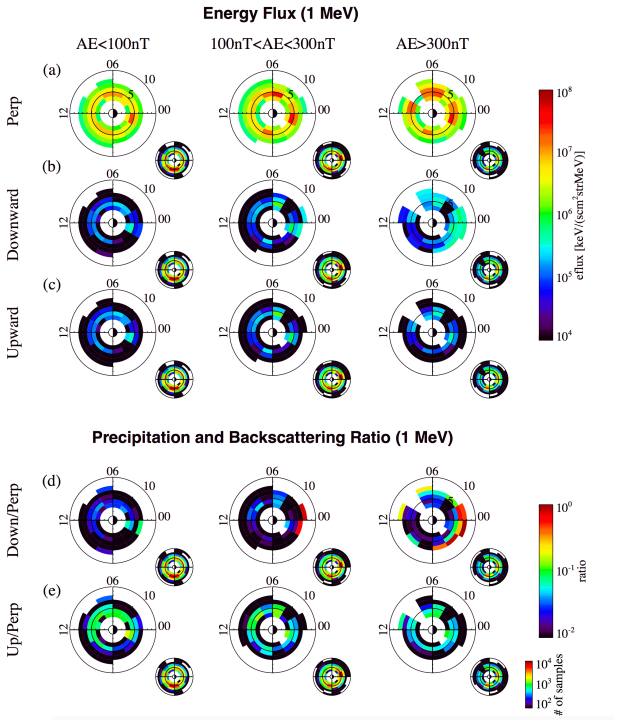

Figure 3. Same as Figure 2, except for 1 MeV energy electrons.

Figure 3 shows the global distribution of 1 MeV electrons. Such high-energy electrons are confined within $L < \sim 8$. Due to the dominant magnetic gradient drift for such high-energy electrons, electron trapped flux (Figure 3a) becomes essentially independent of MLT. For these electrons, the gradient drift time is shorter and the pitch angle scattering timescale gets longer, allowing more particles to drift around the entire magnetic local times. Both the trapped flux (Figure 3a) and precipitating flux (Figure 3b) are enhanced during higher AE. However, the signature of precipitating flux with peaks at high L shells at midnight is different from the trapped flux peaking at lower L shells. The precipitating-to-trapped flux ratio shows the same signature as the precipitation, increasing with increased AE and peaks at midnight at high L shells during stronger geomagnetic activity. This might be related to the current sheet scattering at high L shells. EMIC waves, which have been proposed to be responsible for rapid radiation belt electron loss, are expected to account for the peak 1 MeV precipitation electron flux near the duskside. However, no corresponding peak in the precipitating ratio of 1 MeV electrons is observed on the duskside in our survey.

The backscattering effects decrease dramatically as the energy level increases. This may be due to the fact that low energy electrons are easily scattered in direction while the electrons with higher energy can reach deep into the atmosphere before losing enough energy to be scattered. However, the backscattering ratio of 1 MeV electrons is independent of geomagnetic activity. Besides, it shows a

different signature in the *L*-MLT distribution compared to the precipitating ratio, which needs further examination and is left for future work.

5. Summary and Conclusion

In this study, we have performed a statistical study of the global distribution of energetic electrons at LEO orbit from ELFIN observations (March 2020 – June 2021). Our main findings are summarized below.

1. Pitch angle scattering by whistler mode chorus waves likely accounts for the main features of the low energy electron (60 keV) spatial distribution during various geomagnetic conditions.

2. MeV electron precipitation, which is often proposed to be driven either by current sheet scattering or EMIC wave driven pitch angle scattering, peaks on the nightside at high *L* shells, more consistent with its driver as current sheet scattering in location.

3. The backscattering ratio for 60 keV electrons overall increases during higher AE when the precipitating ratio is high except at high *L* shells (8–10), which needs further detailed examination. The backscattering ratio of 1 MeV electrons is independent of geomagnetic activity. Besides, it shows a different signature in *L*-MLT distribution compared to the precipitating ratio, which needs further examination.

Overall, the low orbit observations with high pitch angle resolution in this study provide new sights into understanding of the physical mechanisms that determine the precipitation rate of energetic electrons in the Earth's magnetosphere.

6. Acknowledgements

This research is supported by the NASA Living With a Star Jack Eddy Postdoctoral Fellowship Program, administered by UCAR's Cooperative Programs for the Advancement of Earth System Science (CPAESS) under award #NNX16AK22G. WL, QM, XS, and LC would like to acknowledge NASA grants of 80NSSC20K0698, 80NSSC19K0845, 80NSSC20K0196, NSF grant of AGS-1847818 and AGS-2019950, and the Alfred P. Sloan Research Fellowship FG-2018-10936. We acknowledge NASA award NNX14AN68G and the NSF award AGS-1242918, and V. Angelopoulos for use of EPD data from the ELFIN Mission.

References

[1] Thorne, R. M. (2010), Radiation belt dynamics: The importance of wave-particle interactions, Geophys. Res. Lett., 37, L22107, doi:10.1029/2010GL044990.

[2] Ripoll, J.-F., Claudepierre, S. G., Ukhorskiy, A. Y., Colpitts, C., Li, X., Fennell, J., & Crabtree, C. (2020). Particle Dynamics in the Earth's Radiation Belts: Review of Current Research and Open Questions. Journal of Geophysical Research: Space Physics, 125, e2019JA026735. https://doi-org.ezproxy.bu.edu/10.1029/2019JA026735.

[3] Büchner, J., & Zelenyi, L. M. (1989). Regular and chaotic charged particle motion in magnetotaillike field reversals: 1. Basic theory of trapped motion. Journal of Geophysical Research, 94(A9), 11821–11842. https://doi-org.ezproxy.bu.edu/10.1029/JA094iA09p11821.

[4] Angelopoulos, V., Tsai, E., Bingley, L. et al. The ELFIN Mission. Space Sci Rev 216, 103 (2020). https://doi-org.ezproxy.bu.edu/10.1007/s11214-020-00721-7.

[5] Lyons, L. R. and Thorne, R. M. (1973). Equilibrium structure of radiation belt electrons. Thorne, Journal of Geophysical Research (1896-1977), 78(13):2142–2149.

[6] Meredith, N. P., Horne, R. B., Isles, J. D., and Green, J. C. (2016), Extreme energetic electron fluxes in low Earth orbit: Analysis of POES E > 30, E > 100, and E > 300 keV electrons, Space Weather, 14, 136– 150, doi:10.1002/2015SW001348.

[7] Li, W., Thorne, R. M., Angelopoulos, V., Bortnik, J., Cully, C. M., Ni, B., LeContel, O., Roux, A., Auster, U., and Magnes, W. (2009), Global distribution of whistler-mode chorus waves observed on the THEMIS spacecraft, Geophys. Res. Lett., 36, L09104, doi:10.1029/2009GL037595.